Classifying the tropospheric precursor patterns of sudden stratospheric warmings

Article

Published Version

AGU PUBLICATIONS

Geophysical Research Letters

RESEARCH LETTER
10.1002/2017GL074611

Key Points:
- The SOM method is used to classify the tropospheric precursor patterns of SSWs
- One of the precursor patterns appears as a mixture of the negative-signed WH pattern and the positive phase of the PNA pattern
- Classifying the precursor patterns could help to better understand the different triggering mechanisms of SSWs

Correspondence to:
M. Bao,
baom@nju.edu.cn

Citation:
Bao, M., X. Tan, D. L. Hartmann, and P. Ceppi (2017), Classifying the tropospheric precursor patterns of sudden stratospheric warmings, *Geophys. Res. Lett.*, *44*, 8011–8016, doi:10.1002/2017GL074611.

Received 16 JUN 2017
Accepted 22 JUL 2017
Accepted article online 26 JUL 2017
Published online 11 AUG 2017

Classifying the tropospheric precursor patterns of sudden stratospheric warmings

Ming Bao[1], Xin Tan[2], Dennis L. Hartmann[3], and Paulo Ceppi[4]

[1]School of Atmospheric Sciences, CMA-NJU Joint Laboratory for Climate Prediction Studies, Nanjing University, Nanjing, China, [2]School of Atmospheric Sciences, Nanjing University, Nanjing, China, [3]Department of Atmospheric Sciences, University of Washington, Seattle, Washington, USA, [4]Department of Meteorology, University of Reading, Reading, UK

Abstract Classifying the tropospheric precursor patterns of sudden stratospheric warmings (SSWs) may provide insight into the different physical mechanisms of SSWs. Based on 37 major SSWs during the 1958–2014 winters in the ERA reanalysis data sets, the self-organizing maps method is used to classify the tropospheric precursor patterns of SSWs. The cluster analysis indicates that one of the precursor patterns appears as a mixed pattern consisting of the negative-signed Western Hemisphere circulation pattern and the positive phase of the Pacific-North America pattern. The mixed pattern exhibits higher statistical significance as a precursor pattern of SSWs than other previously identified precursors such as the subpolar North Pacific low, Atlantic blocking, and the western Pacific pattern. Other clusters confirm northern European blocking and Gulf of Alaska blocking as precursors of SSWs. Linear interference with the climatological planetary waves provides a simple interpretation for the precursors. The relationship between the classified precursor patterns of SSWs and ENSO phases as well as the types of SSWs is discussed.

1. Introduction

Major sudden stratospheric warmings (SSWs) consist of large and rapid temperature increases in the polar stratosphere and a complete reversal of the climatological westerly winds in wintertime. It is known that the occurrence of SSWs is preceded by the enhancement of upward wave fluxes of planetary waves from the troposphere [*Limpasuvan et al.*, 2004; *Polvani and Waugh*, 2004; *Charlton and Polvani*, 2007]. Recent multiyear statistical studies on the precursors of SSWs and polar vortex intensification events (PVIs) have noted that tropospheric blocking in some specific regions and tropospheric variability in the North Pacific can enhance or suppress upward planetary wave propagation and give rise to anomalous stratospheric polar vortices, including SSWs and PVIs [*Martius et al.*, 2009; *Garfinkel et al.*, 2010; *Woollings et al.*, 2010; *Castanheira and Barriopedro*, 2010; *Nishii et al.*, 2010, 2011; *Barriopedro and Calvo*, 2014; *Dai and Tan*, 2016; *Huang et al.*, 2017]. However, these studies have not yet agreed on the tropospheric precursors.

Composite and correlation analysis are used in many of the above studies to detect the tropospheric precursors. A shortcoming of these methods is treating SSWs all together. When explaining why it would be surprising to find a coherent tropospheric precursor pattern, *Limpasuvan et al*. [2005b] argued that the specific geographic source of the anomalous planetary waves for wave numbers 1 or 2 might vary from one SSW event to the next. An early study by *Taguchi* [2008] failed to find significant changes in the frequency of blockings either before or after SSWs. The diversity of blocking precursors may weaken the blocking-SSW statistical linkages [*Woollings et al.*, 2010; *Nishii et al.*, 2011]. Moreover, precursors for regional blocking in the Northern Hemisphere and tropospheric variability in the North Pacific such as the subpolar North Pacific low and the western Pacific (WP) teleconnection pattern focus on the regional signals [*Garfinkel et al.*, 2010; *Nishii et al.*, 2010; *Dai and Tan*, 2016], but neglecting their planetary-scale backgrounds. Although the Pacific-North America (PNA) pattern was suggested to link ENSO variability to the stratospheric polar vortex [e.g. *Garfinkel and Hartmann*, 2008], it is not clear whether the PNA pattern can be regarded as a precursor pattern of SSWs. In view of the above, cluster analysis could provide an alternative framework for classifying different precursors of SSWs without losing the planetary-scale information. Classifying the tropospheric precursor patterns of SSWs could help to better understand the different triggering mechanisms of SSWs.

In this letter, we use the self-organizing maps (SOM) method to perform cluster analysis of the anomalous circulation patterns in the Northern Hemisphere during the growth stage of SSWs. We explore the

precursors and show that one of the precursor patterns appears as a mixed pattern, consisting of a combination of the negative-signed Western Hemisphere (WH) circulation pattern (C2 in *Bao and Wallace* [2015]) and the positive phase of the PNA pattern.

2. Data and Methodology

We combine the four-times-daily 500 hPa geopotential height fields (Z500) from the ERA-40 (1957–1978 [*Uppala et al.*, 2005]) and ERA-Interim (1979–2014 [*Dee et al.*, 2011]) reanalysis data sets to create a continuous 57-winter data set. The data have a 2.5° × 2.5° horizontal resolution. Major SSWs for the period 1958–2014 are chosen according to a SSW Compendium [*Butler et al.*, 2017]. Although 38 SSW events are detected in ERA-40/ERA-Interim reanalysis data set [*Butler et al.*, 2017; *Polvani et al.*, 2017], we remove one SSW event that occurred in February 2002 which is detected in ERA-40 but not in ERA-Interim. Thus, 37 SSWs in ERA reanalysis product are used in this study.

After removing the seasonal cycle averaged over the 57 winters (November–March), the Northern Hemisphere daily average Z500 anomalies are smoothed by a 10 day low-pass filter.

We use the self-organizing maps (SOM) method for cluster analysis [e.g. *Bao and Wallace*, 2015]. In order to assess the distinctiveness of a cluster, we calculate the variance ratio as in *Bao and Wallace* [2015]. The variance ratio is obtained by dividing the squared distance between a cluster's centroid and the centroid of the entire data set by the mean squared distance between the individual maps in that cluster and the centroid of the entire data set.

3. Results

In this study, we identify the precursors of SSWs from the Northern Hemispheric anomalous Z500 field for the period −22 to −10 days. The negative sign indicates days prior to the central date of SSWs. The precursor period in our study is close to the growth stage of SSWs in *Limpasuvan et al*. [2004], but different from the period −10 to 0 days in *Martius et al*. [2009] and *Barriopedro and Calvo* [2014], which is closer to the mature stage of SSWs. The composite (unclassified) precursor of 37 SSWs (Figure 1, top) only shows weak positive anomalies over Northeastern Canada and the North Atlantic and weak negative anomalies over the North Pacific at middle and high latitudes, similar to the composite 250 hPa geopotential height anomalies during the growth stage of SSWs in an earlier study by *Limpasuvan et al*. [2004].

We then use the SOM method to carry out a cluster analysis of the Northern Hemisphere anomalous Z500 field poleward of 20°N averaged over the precursor period −22 to −10 days of 37 SSWs. Figure 1 (middle row) shows the clusters for a 1 × 2 array (typically the number of clusters prescribed in SOM analysis is specified as a two-dimensional array). There are 27 members classified into C2-1 and 10 members into C2-2. However, the variance ratio of C2-1 with the value of 5.1% is very low, meaning that the C2-1 is not very distinctive. Next, we look at the clusters for a 1 × 3 array (Figure 1, bottom row). The variance ratio of each cluster reaches around 20% and each cluster has representative members. Thus, the clusters for a 1 × 3 array satisfy a trade-off between distinctiveness and robustness when considering how many clusters to prescribe in SOM [*Bao and Wallace*, 2015]. The SOM analysis remains similar for slightly different choices of analysis period (−22 to −8 days or −20 to −10 days), but its advantage becomes less clear for periods longer than 17 days for this particular application.

C3-1 to C3-3 represent three types of tropospheric precursor patterns of SSWs. They are significantly different from the SOM regimes identified from all winter days [*Bao and Wallace*, 2015]. C3-1 comprising 14 members is indicative of a northern European blocking pattern along with an upstream wave train from the eastern Pacific to eastern North America. Our result is consistent with previous studies detecting northern European blocking as a precursor of SSWs [*Limpasuvan et al.*, 2004; *Martius et al.*, 2009; *Garfinkel et al.*, 2010; *Woollings et al.*, 2010; *Nishii et al.*, 2011; *Barriopedro and Calvo*, 2014], and it also reveals an accompanying upstream wave train in the precursor pattern.

C3-2 presents a planetary-scale east-west dipole with a negative anomaly in the North Pacific and a positive anomaly in North America and the North Atlantic together with opposite subtropical anomalies, which appears as a westward shifted, negative-signed WH pattern (C2 in *Bao and Wallace* [2015]) or an eastward shifted, positive phase of the PNA pattern. As the negative anomaly extends to the WP and the Far East

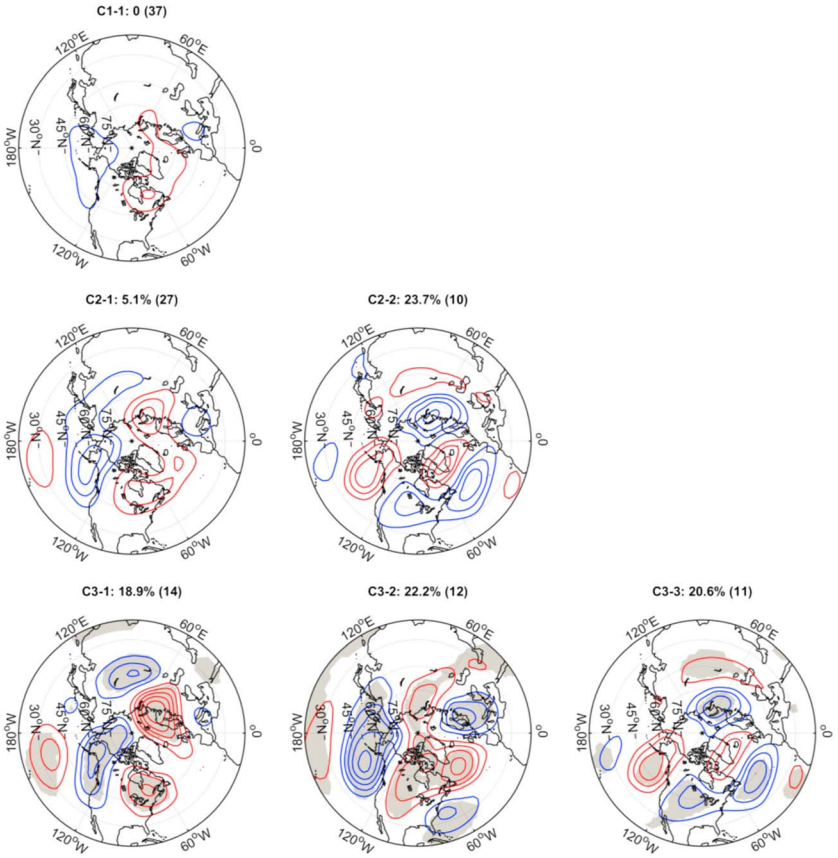

Figure 1. Composite of Z500 anomaly fields during the period −22 to −10 days of (top) 37 SSWs and (middle row) clusters for a 1 × 2 array (note that the number of clusters prescribed in SOM analysis is specified as a two-dimensional array) and (bottom row) clusters for a 1 × 3 array of Z500 anomaly fields averaged over the period −22 to −10 days of 37 SSWs classified in each cluster. Red (blue) contours indicate positive and negative values (interval: 25 m). The variance ratio is denoted by the percentage value, and the number of members in each cluster is shown in parentheses. Gray shading in Figure 1 (bottom row) indicates that the composites are significant beyond the 95% confidence level based on a *t* test.

and the positive anomaly centered over the North Atlantic, C3-2 could be related to the WP pattern, subpolar North Pacific low, and Atlantic blocking precursors suggested in previous studies [*Nishii et al.*, 2010; *Dai and Tan*, 2016; *Garfinkel et al.*, 2010; *Martius et al.*, 2009; *Woollings et al.*, 2010; *Nishii et al.*, 2011; *Barriopedro and Calvo*, 2014]. Nevertheless, here we emphasize the planetary-scale pattern rather than those regional signals as the precursor of SSWs.

We project the daily low-pass filtered anomalous Z500 fields onto the original WH pattern and obtain the normalized WH index. The daily WP, PNA, and North Atlantic Oscillation (NAO) indices are obtained by projecting daily low-pass filtered anomalous Z500 fields onto the WP, PNA, and NAO patterns, which are produced from the regression of monthly mean Z500 anomalies onto the NOAA monthly WP, PNA, and NAO indices, respectively. We also define three indices for the area-weighted averaged daily low-pass filtered Z500 anomalies divided by their respective standard deviations during November–March over the Pacific low (150°E–130°W, 40°N–70°N), the Atlantic high (60°W–10°W, 40°N–65°N), and the Gulf of Alaska high (160°W–130°W, 40°N–65°N).

Figures 2a–2c shows the 7 day running mean indices for the WP pattern, the WH pattern, the PNA pattern, the Pacific low, and the Atlantic high for the period −30 to 0 days of 12 SSWs classified in C3-2. Using 7 day running means only makes the plots look smoother, but the visual appearance is not sensitive to the alternative choice of a 9 day or 11 day running mean. We have put confidence limits on the composite mean values in Figure 2, based on the unsmoothed daily data. All the 12 SSWs show persistent, negative WH indices and

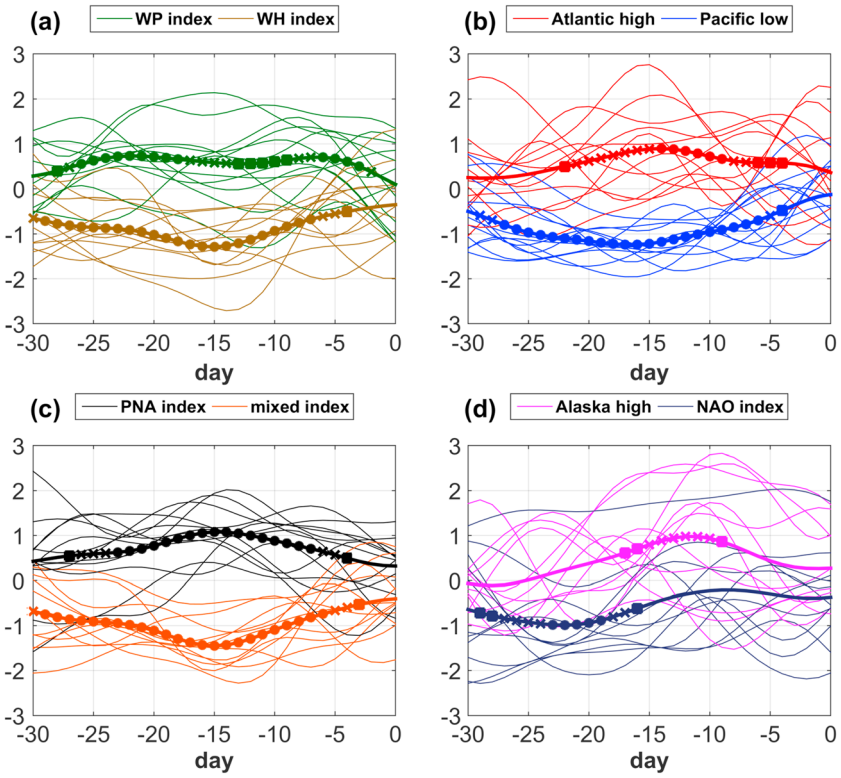

Figure 2. Seven day running mean indices during the period −30 to 0 days for (a) the WP pattern (green) and the WH pattern (brown), (b) the Atlantic high (red) and the Pacific low (blue), (c) the PNA pattern (black) and the mixed pattern (orange) of 12 SSWs classified in C3-2, and for (d) the Alaska high (magenta) and the NAO (navy) of 11 SSWs classified in C3-3. Composites of the 7 day running mean indices are denoted by the thick lines. Squares, crosses, and dots denote 90%, 95%, and 99% confidence limits on the composite mean values, respectively.

positive PNA indices during the growth stage of SSWs. The composite for the WH indices and the PNA indices shows a higher confidence level than that for the WP indices (Figures 2a and 2c), and the WH indices precede the PNA indices. Contrasting the Pacific low and the Atlantic high indices, both of them contribute to the precursor pattern of SSWs, but the Pacific low plays a more important role (Figure 2b). When we project the daily low-frequency anomalous Z500 fields onto a mixed pattern calculated as the average of the negative-signed WH pattern and the positive phase of the PNA pattern, the composite for the mixed index shows the highest level of significance (Figure 2c).

C3-3 is characterized by a local blocking high over the Gulf of Alaska and projects negatively upon the NAO pattern (Figure 1, bottom row). The Gulf of Alaska high in C3-3 is similar to the blocking frequency composites in *Martius et al.* [2009], who found significant blocking occurrence over the northeastern Pacific for both the periods −10 to 0 days and −20 to −10 days for splitting SSWs. The corresponding time series in Figure 2d indicate that the negative NAO appears earlier (before day −16) and the Gulf of Alaska blocking appears later (after day −17), and both of them are not as significant as the indices of C3-2 precursor.

A detailed study of the dynamical connection between the three types of tropospheric precursors and SSWs will be investigated in the future. Here we compare the precursors and climatological planetary waves to make a simple interpretation. Figure 3 shows the three clusters superimposed on the climatological stationary wave-1 and wave-2 components of the Z500 field, respectively. The Z500 anomalies of each cluster that are in phase with the climatological wave-1 and wave-2 components are effective in deepening them by constructive interference, and vice versa. Therefore, it is shown from the map correlations in Figure 3 that C3-1 and C3-2 mainly deepen the climatological wave-1 amplitudes, and C3-3 deepens the climatological wave-2 amplitudes. All three precursors constructively interfere with the climatological planetary wave-1 or wave-2 and thus favor the occurrence of SSWs.

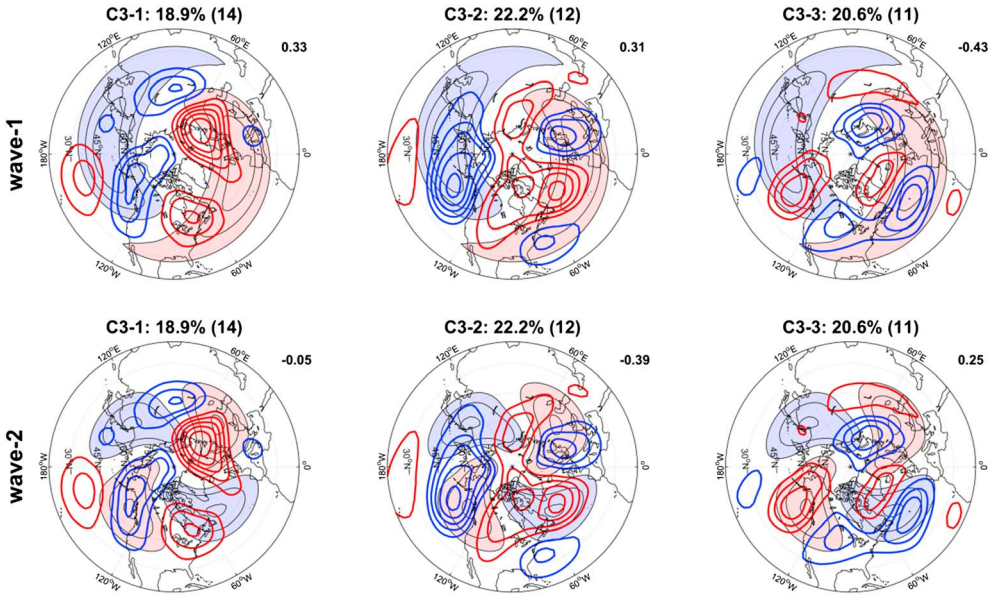

Figure 3. Composites of Z500 anomalies (contours) for C3-1, C3-2, and C3-3, superimposed on the climatological planetary (top row) wave-1 and (bottom row) wave-2 height fields (shading). Red and blue contours are same as in Figure 1. Red (blue) shading indicates positive (negative) values (interval: 25 m). The value of the spatial correlation coefficients between C3-1–C3-3 and the climatological planetary waves is shown at the top right corner of each plot.

4. Discussion

In this study, we identify the tropospheric precursor patterns of SSWs using the SOM clustering method. Classifying the precursor patterns could help to better understand the different triggering mechanisms of SSWs. One of the three types of precursor pattern appears as a mixture of the negative-signed WH pattern and the positive phase of the PNA pattern, which constructively interferes with the climatological planetary wave-1 and favors the occurrence of SSWs. A novel aspect of our study is the finding that this mixed pattern can be considered as a tropospheric precursor pattern when predicting SSWs.

Previous studies of ENSO modulation on SSWs have given rise to some confusion [*Taguchi and Hartmann*, 2006; *Butler and Polvani*, 2011; *Garfinkel et al.*, 2012; *Barriopedro and Calvo*, 2014; *Dai and Tan*, 2016; *Polvani et al.*, 2017]. *Butler and Polvani* [2011] found that major SSWs occur with equal probability during El Niño and La Niña winters. Recently, *Polvani et al*. [2017] revisited the findings of *Butler and Polvani* [2011], and their new results based on an updated sea surface temperature data set conclude that El Niño appears to enhance the occurrence of SSWs. Referring to *Butler et al*. [2017], their table from http://www.esrl.noaa.gov/csd/groups/csd8/sswcompendium/, and *Polvani et al*. [2017, Table S2], here we list in Table 1 the number of SSWs for each ENSO phase and each type of precursor. An interesting result that emerges in Table 1 is that ENSO modulation of the occurrence of SSWs is due to the precursor of C3-2, viz., SSWs associated with the C3-2 pattern precursor tends to occur in El Niño winters.

Although separate composites for displacement and splitting SSWs have shown distinct precursors associated with regional blocks [*Charlton and Polvani*, 2007; *Martius et al.*, 2009], we find a higher occurrence of displacement SSWs for C3-2 and splitting SSWs for C3-3 (Table 1). Owing to the limited SSWs samples and

Table 1. The Number of Classified SSWs According to C3-1–C3-3 Precursors During 1958–2014 for the Different ENSO Phases and Different Types of SSWs

	ENSO Phases			Types of SSWs	
	El Niño	La Niña	Neutral	Splitting	Displacement
C3-1	4	5	5	7	7
C3-2	8	2	2	5	7
C3-3	4	3	4	7	4

the relatively small difference, the relationship between classification of the precursors and the types of SSWs remains to be confirmed.

The results bring up the question whether the WH pattern is a precursor of extreme PVIs. Compositing tropospheric patterns during the growth stage of PVIs shows a wave train that projects positively onto the WH pattern [*Limpasuvan et al.*, 2005a; *Huang et al.*, 2017]. This suggests that a pattern associated with the WH pattern could be a major precursor of PVIs. A similar cluster analysis will be performed to validate the hypothesis and identify different types of tropospheric precursors of PVIs in a companion study.

Acknowledgments
We thank two anonymous reviewers for their very useful comments on the manuscript. The ERA-40 and ERA-Interim atmospheric reanalysis data sets were provided by the European Center for Medium-Range Weather Forecasts (https://www.ecmwf.int/en/research/climate-reanalysis/browse-reanalysis-datasets). M.B. and X.T. were supported by the National Natural Science Foundation of China (grants 41675048, 41275054, and 41330420). D.L.H. and P.C. were supported by the National Science Foundation under grant AGS-0960497. P.C. was additionally supported by the ERC Advanced Grant "ACRCC."

References

Bao, M., and J. M. Wallace (2015), Cluster analysis of Northern Hemisphere wintertime 500-hPa flow regimes during 1920–2014, *J. Atmos. Sci.*, *72*, 3597–3608, doi:10.1175/JAS-D-15-0001.1.

Barriopedro, D., and N. Calvo (2014), On the relationship between ENSO, stratospheric sudden warmings, and blocking, *J. Clim.*, *27*, 4704–4720, doi:10.1175/JCLI-D-13-00770.1.

Butler, A. H., and L. M. Polvani (2011), El Niño, La Niña, and stratospheric sudden warmings: A reevaluation in light of the observational record, *Geophys. Res. Lett.*, *38*, L13807, doi:10.1029/2011GL048084.

Butler, A. H., J. P. Sjoberg, D. J. Seidel, and K. H. Rosenlof (2017), A sudden stratospheric warming compendium, *Earth Syst. Sci. Data*, *9*, 63–76, doi:10.5194/essd-9-63-2017.

Castanheira, J. M., and D. Barriopedro (2010), Dynamical connection between tropospheric blockings and stratospheric polar vortex, *Geophys. Res. Lett.*, *37*, L13809, doi:10.1029/2010GL043819.

Charlton, A. J., and L. M. Polvani (2007), A new look at stratospheric sudden warmings. Part I: Climatology and modeling benchmarks, *J. Clim.*, *20*, 449–469, doi:10.1175/JCLI3996.1.

Dai, Y., and B. Tan (2016), The western Pacific pattern precursor of major stratospheric sudden warmings and the ENSO modulation, *Environ. Res. Lett.*, *11*, doi:10.1088/1748-9326/aa538a.

Dee, D. P., et al. (2011), The ERA-Interim reanalysis: Configuration and performance of the data assimilation system, *Q. J. R. Meteorol. Soc.*, *137*, 553–597, doi:10.1002/qj.828.

Garfinkel, C. I., and D. L. Hartmann (2008), Different ENSO teleconnections and their effects on the stratospheric polar vortex, *J. Geophys. Res.*, *113*, D18114, doi:10.1029/2008JD009920.

Garfinkel, C. I., D. L. Hartmann, and F. Sassi (2010), Tropospheric precursors of anomalous northern hemisphere stratospheric polar vortices, *J. Clim.*, *23*, 3282–3299, doi:10.1175/2010JCLI3010.1.

Garfinkel, C. I., A. H. Butler, D. W. Waugh, M. M. Hurwitz, and L. M. Polvani (2012), Why might stratospheric sudden warmings occur with similar frequency in El Niño and La Niña winters?, *J. Geophys. Res.*, *117*, D19106, doi:10.1029/2012JD017777.

Huang, J., W. Tian, J. Zhang, Q. Huang, H. Tian, and J. Luo (2017), The connection between extreme stratospheric polar vortex events and tropospheric blockings, *Q. J. R. Meteorol. Soc.*, *143*, 1148–1164, doi:10.1002/qj.3001.

Limpasuvan, V., D. W. J. Thompson, and D. L. Hartmann (2004), The life cycle of the Northern Hemisphere sudden stratospheric warmings, *J. Clim.*, *17*, 2584–2596, doi:10.1175/1520-0442(2004)017<2584:TLCOTN>2.0.CO;2.

Limpasuvan, V., D. L. Hartmann, D. W. J. Thompson, K. Jeev, and Y. L. Yung (2005a), Stratosphere-troposphere evolution during polar vortex intensification, *J. Geophys. Res.*, *110*, D24101, doi:10.1029/2005JD006302.

Limpasuvan, V., D. W. J. Thompson, and D. L. Hartmann (2005b), Reply, *J. Clim.*, *18*, 2778–2780, doi:10.1175/JCLI3444.1.

Martius, O., M. Polvani, and H. C. Davies (2009), Blocking precursors to stratospheric sudden warming events, *Geophys. Res. Lett.*, *36*, L14806, doi:10.1029/2009GL038776.

Nishii, K., H. Nakamura, and Y. J. Orsolini (2010), Cooling of the wintertime Arctic stratosphere induced by the western Pacific teleconnection pattern, *Geophys. Res. Lett.*, *37*, L13805, doi:10.1029/2010GL043551.

Nishii, K., H. Nakamura, and Y. J. Orsolini (2011), Geographical dependence observed in blocking high influence on the stratospheric variability through enhancement and suppression of upward planetary-wave propagation, *J. Clim.*, *24*, 6408–6423, doi:10.1175/JCLI-D-10-05021.1.

Polvani, L. M., and D. W. Waugh (2004), Upward wave activity flux as a precursor to extreme stratospheric events and subsequent anomalous surface weather regimes, *J. Clim.*, *17*, 3548–3554, doi:10.1175/1520-0442(2004)017<3548:UWAFAA>2.0.CO;2.

Polvani, L. M., L. Sun, A. H. Butler, J. H. Richter, and C. Deser (2017), Distinguishing stratospheric sudden warmings from ENSO as key drivers of wintertime climate variability over the North Atlantic and Eurasia, *J. Clim.*, *30*, 1959–1969, doi:10.1175/JCLI-D-16-0277.1.

Taguchi, M. (2008), Is there a statistical connection between stratospheric sudden warming and tropospheric blocking events?, *J. Atmos. Sci.*, *65*, 1442–1454, doi:10.1175/2007JAS2363.1.

Taguchi, M., and D. L. Hartmann (2006), Increased occurrence of stratospheric sudden warmings during El Niño simulated by WACCM, *J. Clim.*, *19*, 324–332, doi:10.1175/JCLI3655.1.

Uppala, S. M., et al. (2005), The ERA-40 re-analysis, *Q. J. R. Meteorol. Soc.*, *131*, 2961–3012, doi:10.1256/qj.04.176.

Woollings, T., A. Charlton-Perez, S. Ineson, A. G. Marshall, and G. Masato (2010), Associations between stratospheric variability and tropospheric blocking, *J. Geophys. Res.*, *115*, D06108, doi:10.1029/2010JD012742.